Robotica (2009) volume 27, pp. 1075–1089. © Cambridge University Press 2009
doi:10.1017/S0263574709005499

Development and target following of vision-based autonomous robotic fish

Yonghui Hu*, Wei Zhao, Guangming Xie and Long Wang

Intelligent Control Laboratory, Department of Mechanics and Space Technologies, College of Engineering, Peking University, Beijing 100871, P. R. China

(Received in Final Form: February 10, 2009. First published online: March 10, 2009)

SUMMARY

A novel ostraciiform swimming, vision-based autonomous robotic fish is developed in this paper. Its feasibility and capability are shown by implementing a dynamic target following task in a swimming pool. Inspired by boxfish that is highly stable and fairly maneuverable, the robotic fish is designed and constructed by locating multiple propulsors peripherally around a rigid body. Swimming locomotion of the robotic fish is achieved through harmonic oscillations of the tail and pectoral fins. The forces and moments acting on the fins and body are analyzed and the governing motion equations are derived. Through coordinating the movements of the propulsors, several typical swimming patters are empirical designed and realized. A digital camera is integrated in the robotic fish, and the visual information is processed with the embedded microcontroller. To treat the degradation of underwater image, a continuously adaptive mean shift (Camshift) algorithm is modified to keep visual lock on the moving target. A fuzzy logic controller is designed for motion regulation of a hybrid swimming pattern, which employs synchronized pectoral fins for thrust generation and tail fin for steering. A simple target following task is designed via an autonomous robotic fish swimming after a manually controlled robotic fish with fixed distance. The swimming performance of the robotic fish is tested and the effectiveness of the proposed target following method is verified experimentally.

KEYWORDS: Autonomous underwater vehicles; Biomimetic robotic fish; Swimming pattern; Visual tracking; Target following.

1. Introduction

Biorobotic autonomous underwater vehicles (AUVs) have become one of the hot research topics in the last decade.[1] The driving motivation for this research is to unveil the underlying biological principles of marine propulsion and maneuvering and to incorporate this knowledge into nautical engineering practice. Contemporary AUV technology will benefit from this study for enhanced swimming performance such as high efficiency, great agility, station-keeping ability, and reduced detection.

* Corresponding author. E-mail: huyhui@gmail.com

Majority of research work in this area have focused on fish-like swimming and their engineered counterpart, robotic fish. As one of the oldest creatures on this planet, fish have evolved an astonishing level of swimming abilities throughout the ages of natural selection. By means of active and passive manipulation of flow around the body and fins, fish generate propulsive and maneuvering forces efficiently, while reducing the resistance effectively.[2] Based upon the propulsive structures employed for locomotion, the swimming of fish can be classified into two categories: body and/or caudal fin (BCF) swimming and median and/or paired fin (MPF) swimming.[3] BCF swimmers generate thrust by bending their bodies into a backward moving propulsive wave that extends from the nose to caudal fin. The variation in wavelength and the amplitude envelope of the propulsive wave further split the BCF swimming into several subcategories, from anguilliform swimming that involves the undulation of the whole body, the carangiform swimming in which the undulation is confined to the last third of the body length, to the ostraciiform swimming characterized by the pendulum-like oscillation of the caudal fin. The MPF swimming is also categorized into different types according to the propulsors that contribute to thrust generation and the extent to which propulsion is based on undulatory versus oscillatory motion. Recent reviews[4–6] provide thorough investigations on advances in morphology, kinematics, and hydrodynamics of swimming fish.

With the increasing understanding of how fish swim and the progress in supporting technologies, various swimming machines that mimic the morphology and locomotion of fish have been built around the world. The first robotic fish is the well-known RoboTuna developed by Triantafyllou and co-workers[7,8] in 1994. Extensive experiments conducted on RoboTuna demonstrated that drag was significantly reduced while the robot being towed at constant velocity through water, which provided a solid experimental and theoretical foundation for subsequent research in this field. Anderson and Kerrebrock[9] built the mission-scale, autonomous underwater vehicle VCUUV that utilizes vorticity control mechanisms for propulsion and maneuvering. Mason and Burdick[10] constructed a three-link carangiform swimmer for prediction of thrust generation with flapping tail. Hirata[11] realized a series of robotic fish with different design objectives, from PF200 for up-down motion, PF300 for turning performance, to PF700 for high-speed swimming. Liu *et al.*[12] developed autonomously swimming robotic fish

based on biologically inspired behavior-based approach. Kato[13] developed a pectoral fin-driven robotic fish called "BlackBass" for precise maneuvering control. To mimic the actual flexible fin of real fish, Low[14] designed a fin-like mechanism that functions like a flexible membrane. Previously, the authors[15] developed a module-based robotic fish that propels either with the posterior flexible body and oscillating tail foil or by the combined pitching and heaving motion of the two-degree-of-freedom (2-DOF) pectoral fins. In addition, conceptual design of a biorobotic AUV that employs pectoral fins for low-speed swimming, precise maneuvering, and station holding was suggested by a team of biologists and engineers in a workshop organized by Office of Naval Research (ONR) of America.[16] Excellent reviews regarding the state of art biorobotic AUVs are provided in refs. [1, 17].

Control of robotic fish requires modeling of the fluid dynamics of momentum transferring for thrust generation. Since the mechanisms of flow body interaction are typically quite complex, no analytical methods are available for controller design. Most designers of robotic fish employ greatly simplified, low fidelity hydrodynamic models or kinematic models of fish body during swimming. Kelly *et al.*[18] developed a planar model for carangiform swimming based on a set of reduced Euler–Lagrange equations that describe the interaction of the body and the surrounding fluid with forcing from a single point vortex, and used geometric nonlinear control methods for motion generation. McIsaac and Ostrowski[19] designed various open-loop locomotive gaits for eel-like robot based on planar dynamic model using perturbation analysis. Morgansen *et al.*[20] developed a dynamic model that takes into account the added mass effect and quasi-static lift and drag, and used geometric nonlinear control theory for trajectory tracking of a fin-actuated underwater vehicle. Barrett *et al.*[8] determined experimentally the power-optimal motion of RoboTuna based on the kinematic model of swimming fish using genetic algorithm. Yu *et al.*[21] optimized numerically the relative link lengths of multi-linked robotic fish to find the discretized traveling wave that best matches the shape of fish body. To deal with the complexity of swimming hydrodynamics, fuzzy rule-based control method is used by Kato[13] in performing rendezvous and docking with an underwater post in water currents and by Zhang *et al.*[22] in coordinated transport by multiple robotic fish in aquatic environment.

Most studies of robotic fish have focused on carangiform swimming for its high speed and efficiency, and ostraciiform swimming fish have classically been considered to be slow swimmers. However, recent studies reveal that ostraciiform swimmers like boxfish (see Fig. 1) can maintain a high level of dynamic stability to swim smoothly through turbulent waters and exhibit excellent maneuverability, which are desirable characteristics for AUVs.[23,24] Growing interests in building robotic fish mimicing ostraciiform swimming have been spurred.[25,26] This paper presents a novel free-swimming robotic fish that utilizes ostraciiform swimming mode for cruise and maneuver. A pair of pectoral fins and a tail fin are implemented around a rigid box-like fish body. The use of multiple peripherally located control surfaces allows realization of various swimming patterns and high maneuverability, while the boxy rigid body ensures the stability of the underwater robot. Swimming machines with such locomotive characteristics can be used in practical applications that require operations in cluttered environment and unsteady flow such as coral reef monitoring, ship wreck exploration, and in-pipe inspections. To realize autonomous operation, the robotic fish is equipped with a CMOS camera. The huge volume of underwater visual information can be processed with the onboard processor and vision-based underwater tasks can be performed. To the best of our knowledge, no vision-based autonomous robotic fish have been realized before and only robotic fish with simpler sensor like pressure sensor, infrared sensor have been designed.[12] The contribution of this paper lies in two aspects: (1) the design of an ostraciiform swimming robotic fish that exhibits high stability, high maneuverability, and various swimming patterns and (2) the implementation of underwater vision-based target following, where color-based adaptive mean shift algorithm is used for object identification and fuzzy logic controller for motion regulation.

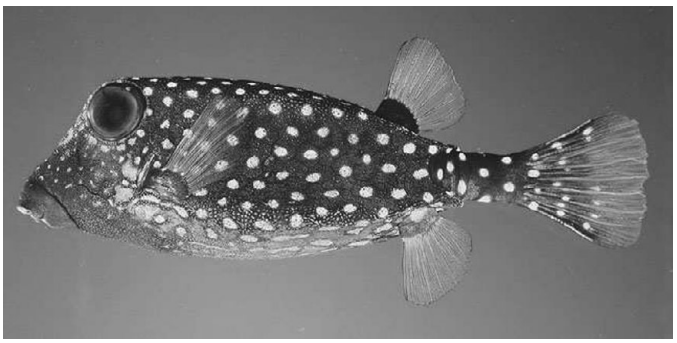

Fig. 1. Photograph of a spotted boxfish.

In the rest of the paper, we proceed as follows: Section 2 describes the mechanical, electrical, and software design of the robotic fish. Section 3 presents basic motion control, dynamic analysis, and typical swimming patterns of the robotic fish. The algorithms for underwater target following are addressed in Section 4. In Section 5, experiments with the robotic fish are conducted. Finally, we conclude the paper with an outline of future work in Section 6.

2. Design of Robotic Fish Prototype

The robotic fish is a highly sophisticated mechatronic system that incorporate mechanics, electronics, software, and control techniques. Design details of the prototype will be phrased in the following three aspects.

2.1. Mechanical design

Modeled after boxfish that is characterized by inflexible body and utilizes MPF mode for propulsion and caudal oscillations as auxiliary locomotion means, the robotic fish consists of a rigid main body, a pair of pectoral fins, and a caudal fin. The main body, which is roughly a rectangular, waterproofed hull, provides housings for the power, electronics, and actuators. Each propulsor can perform 1-DOF movements and is actuated by a servomotor (Hitec HS-5955TG) that is fixed on the bottom chassis. The reciprocatory rotation of the

https://doi.org/10.1017/S0263574709005499 Published online by Cambridge University Press

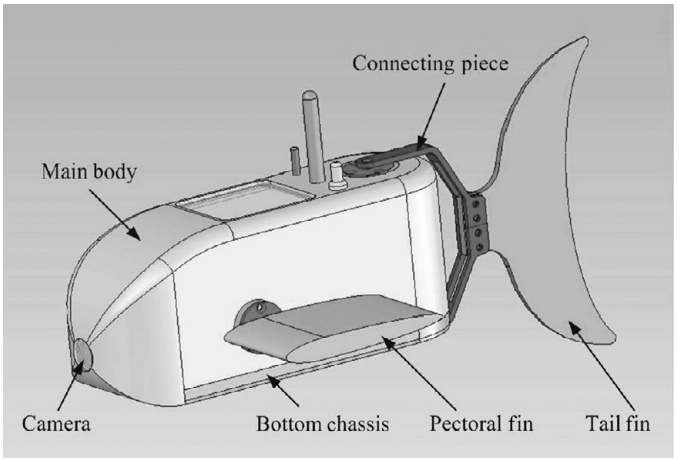

Fig. 2. Mechanical configurations of the robotic fish.

servomotors is transmitted to the outside through dynamic sealing structure filled with grease. The pectoral fins with the approximate shape of NACA-0012 profile are attached to the joints on the side, and the lunate tail fin is linked to the vertical joints with connecting pieces. The rotatory range of the tail fin is limited to $\pm 90^\circ$, while that of the pectoral fins is expanded to $\pm 180^\circ$ through transmission of gear sets of 2:1 ratio. A pinhole CMOS camera, as the only exteroceptive sensor is installed at the mouth position with a transparent window glued to the hull for waterproof purpose. For most fishes, the center of mass is located above the center of buoyancy and as a result they are hydrostatically unstable.[27] However, it is hard for robotic fish to generate the necessary trimming forces and powered correction forces to stabilize and hold posture, therefore the robotic fish is designed to be hydrostatically stable through lower placement of the mass center. The density of the robotic fish has been designed to be close to that of water through careful calculations, so that little trimming weight or foam can be added to accomplish neutral buoyancy. Figure 2 shows the mechanical configurations of the robotic fish.

2.2. Electronics and sensor

The robotic fish is designed for autonomous operation such that it is equipped with onboard power, embedded processor, image sensor (OV7620 from OmniVision), and a duplex wireless communication module (GW100B from Unitel Pty Ltd.) as the user interface for human–robot interaction. Four rechargeable Ni–Cd cells of 2700 mAh capacity provide the robotic fish about 1 h power autonomy. The control unit is a microcontroller S3C2440 that incorporates a high-performance 32-bit RISC, ARM920T CPU core running at 400 MHz and a wide range of peripherals from Samsung Electronics. The onboard memory includes 64MB SDRAM used during program execution and 64MB Nand Flash for permanent data and code storage. The microcontroller captures image data in YCrCb 4:2:2 format at 320×240 resolution and does real-time image processing for perception of the environment. Three PWM (Pulse Width Modulation) signals are generated by the microcontroller to control the motion of the joints. Figure 3 illustrates hardware architecture of the control system.

2.3. Software

The software running on the robotic fish is comprised of two parts: a boot program named U-boot (universal bootloader) and the application code. U-boot runs immediately when the robotic fish powers up, and then waits a few seconds for the user to update application code through the wireless communication module. By default, U-boot will transfer the control to the application code that is already stored in Nand Flash memory if the user did not interrupt. The use of U-boot greatly simplifies and accelerates the Flash burning process, which conventionally involves taking apart the bottom chassis, pulling out cables, and resealing of the fish body.

3. Dynamic Analysis and Swimming Locomotion Control

3.1. Basic motion control

The robotic fish swims by oscillatory movements of the tail and pectoral fins. Since sinusoidal signals can generate smooth oscillations and allow flexible and easy adjustment of joint angles, we model the swimming locomotion as sinusoidal variation of the robot's joint angles. Each joint of the robotic fish oscillates in a harmonic manner according to the following equation:

$$\theta(t) = \phi + A \sin(2\pi f t + \varphi), \tag{1}$$

where $\theta(t)$ is the target angular position at time t, ϕ denotes the angular offset, A represents the oscillatory amplitude of the joint angle, f indicates the frequency, and φ is the phase difference between the left pectoral fin, the right pectoral fin, and the tail fin. The magnitude of thrust generated by the propulsor can be adjusted by modulating the value of the frequency f and the amplitude A, while its direction is determined by the angular offset ϕ. The phase difference φ couples the joints for swimming behavior design. The motion behavior of the robotic fish is governed by a total of 12 parameters. For convenience of description, suffix "t" will be used to represent the parameters of tail fin, suffixes "lp" and "rp" the parameters of left and right pectoral fin, respectively. When the left and right pectoral fins move synchronously, suffix "p" will be used to represent the common parameters of both pectoral fins.

3.2. Dynamic analysis

The dynamic analysis of the robotic fish consists of writing and solving the equations that govern the translational and rotational motions of the robot in 3D space. To facilitate the description, two coordinate frames are defined, namely the body-fixed coordinate frame xyz and the earth-fixed inertial coordinate frame XYZ. The body reference frame xyz has its origin at the center of mass of the robot, its x-axis pointing forward, its y-axis pointing through the right-hand side, and its z-axis pointing downward. The robotic fish can both translate along and rotate about each axis of the body frame, obtaining the following 6-DOF: surge, sway, heave, roll, pitch, and yaw. Figure 4 illustrates the coordinate frames and the 6-DOF of the robotic fish. The body-fixed coordinate

https://doi.org/10.1017/S0263574709005499 Published online by Cambridge University Press

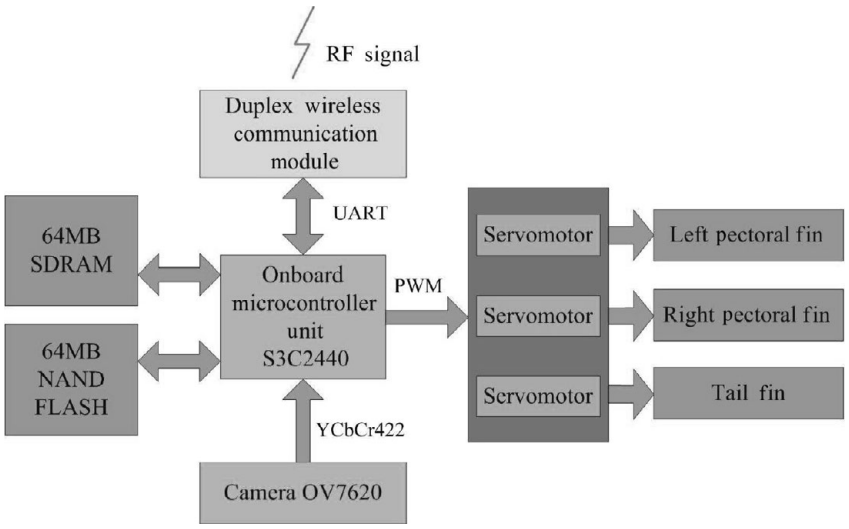

Fig. 3. Hardware architecture of the control system.

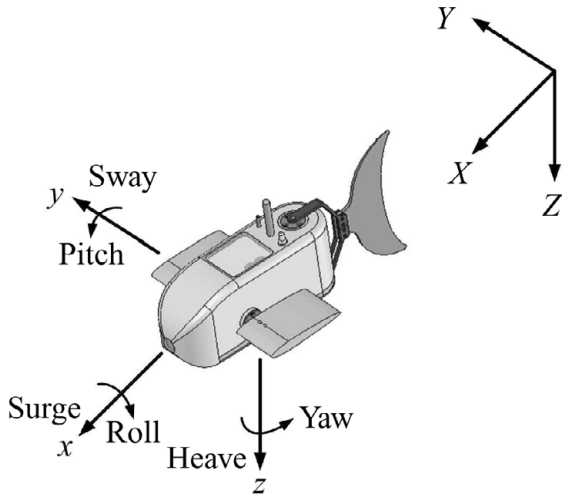

Fig. 4. Coordinate frames and robot motions.

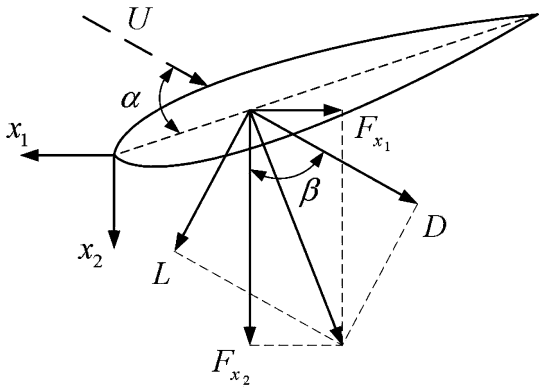

Fig. 5. Forces on an oscillating foil.

components of robot translational velocity are denoted as $[u \quad v \quad w]^T$ and the components of angular velocity with respect to body frame are denoted as $[p \quad q \quad r]^T$. The motion equations of the robotic fish will be derived in the body frame in the sequel, and the dynamics in inertial frame can be obtained through a series of transformations.[28]

To characterize every detail of the hydrodynamics of the robotic fish is a daunting task, therefore a set of assumptions has to be made in order to develop a simplified hydrodynamic model. We suppose that the robotic fish swims in an infinite volume of incompressible and irrotational fluid, thus allowing the neglection of the effect of the vortices shed by the body and fins, and the effect of nearby walls and surfaces. Moreover, the robotic fish is assumed to be neurally buoyant and the center of mass coincides with the volumetric center of the robot, so that the hydrostatic (gravitational and buoyancy) forces and moments are zero. After the above simplifications, the forces and moments acting on the robotic fish are the hydrodynamic forces generated by its constituent components, i.e. the rigid body and the three propulsors.

The tail and pectoral fins, which provide the propulsive force with 1-DOF oscillation, can be modeled as oscillating foils. Consider, as shown in Fig. 5, an oscillating foil moving at velocity U relative to the inflow fluid in reference frame x_1x_2. The angle between the direction of flow impinging on the foil and x_2 axis is denoted as β, while the direction of flow relative of the foil is called the angle of attack and denoted as α. The forces generated by the foil are lift and drag, perpendicular and parallel to the fluid flow, respectively. The magnitudes of lift L and drag D can be calculated as follows[29]:

$$L = \frac{1}{2}\rho A C_L U^2, \tag{2}$$

$$D = \frac{1}{2}\rho A C_D U^2, \tag{3}$$

where ρ is the density of water, A is the planform area of the foil, C_L and C_D are lift and drag coefficients that depend on the angle of attack α and can be determined with experimental techniques. Decomposing the lift and drag forces along x_1 and x_2 directions, the following expressions for the x_1 and x_2 components of the force can be obtained:

$$F_{x_1} = L\cos\beta - D\sin\beta, \tag{4}$$

https://doi.org/10.1017/S0263574709005499 Published online by Cambridge University Press

$$F_{x_2} = L\sin\beta + D\cos\beta. \tag{5}$$

Based on the above analysis, the forces on the tail fin oscillating in xy plane of body reference frame can be calculated as

$$\vec{F}_{\mathrm{t}} = \begin{bmatrix} L_{\mathrm{t}}\cos\beta_{\mathrm{t}} - D_{\mathrm{t}}\sin\beta_{\mathrm{t}} \\ L_{\mathrm{t}}\sin\beta_{\mathrm{t}} + D_{\mathrm{t}}\cos\beta_{\mathrm{t}} \\ 0 \end{bmatrix}. \tag{6}$$

The forces on the tail fin create moments on the center of mass of the robotic fish. The moment produced by tail fin can be obtained as follows:

$$\vec{M}_{\mathrm{t}} = \begin{bmatrix} x_{\mathrm{t}} \\ y_{\mathrm{t}} \\ z_{\mathrm{t}} \end{bmatrix} \times \begin{bmatrix} L_{\mathrm{t}}\cos\beta_{\mathrm{t}} - D_{\mathrm{t}}\sin\beta_{\mathrm{t}} \\ L_{\mathrm{t}}\sin\beta_{\mathrm{t}} + D_{\mathrm{t}}\cos\beta_{\mathrm{t}} \\ 0 \end{bmatrix} \tag{7}$$

$$= \begin{bmatrix} -z_{\mathrm{t}}(L_{\mathrm{t}}\sin\beta_{\mathrm{t}} + D_{\mathrm{t}}\cos\beta_{\mathrm{t}}) \\ z_{\mathrm{t}}(L_{\mathrm{t}}\cos\beta_{\mathrm{t}} - D_{\mathrm{t}}\sin\beta_{\mathrm{t}}) \\ x_{\mathrm{t}}(L_{\mathrm{t}}\sin\beta_{\mathrm{t}} + D_{\mathrm{t}}\cos\beta_{\mathrm{t}}) - y_{\mathrm{t}}(L_{\mathrm{t}}\cos\beta_{\mathrm{t}} - D_{\mathrm{t}}\sin\beta_{\mathrm{t}}) \end{bmatrix}, \tag{8}$$

where x_{t}, y_{t}, and z_{t} are coordinate components of the distance from the center of propulsive force on tail fin to the center of mass of the robotic fish in body-fixed reference frame. Similarly, the forces and moments produced by left and right pectoral fins that oscillate in xz plane are given by

$$\vec{F}_{\mathrm{lp}} = \begin{bmatrix} L_{\mathrm{lp}}\cos\beta_{\mathrm{lp}} - D_{\mathrm{lp}}\sin\beta_{\mathrm{lp}} \\ 0 \\ L_{\mathrm{lp}}\sin\beta_{\mathrm{lp}} + D_{\mathrm{lp}}\cos\beta_{\mathrm{lp}} \end{bmatrix}, \tag{9}$$

$$\vec{F}_{\mathrm{rp}} = \begin{bmatrix} L_{\mathrm{rp}}\cos\beta_{\mathrm{rp}} - D_{\mathrm{rp}}\sin\beta_{\mathrm{rp}} \\ 0 \\ L_{\mathrm{rp}}\sin\beta_{\mathrm{rp}} + D_{\mathrm{rp}}\cos\beta_{\mathrm{rp}} \end{bmatrix}, \tag{10}$$

$$\vec{M}_{\mathrm{lp}} = \begin{bmatrix} y_{\mathrm{lp}}(L_{\mathrm{lp}}\sin\beta_{\mathrm{lp}} + D_{\mathrm{lp}}\cos\beta_{\mathrm{lp}}) \\ -x_{\mathrm{lp}}(L_{\mathrm{lp}}\sin\beta_{\mathrm{lp}} + D_{\mathrm{lp}}\cos\beta_{\mathrm{lp}}) + z_{\mathrm{lp}}(L_{\mathrm{lp}}\cos\beta_{\mathrm{lp}} - D_{\mathrm{lp}}\sin\beta_{\mathrm{lp}}) \\ -y_{\mathrm{lp}}(L_{\mathrm{lp}}\cos\beta_{\mathrm{lp}} - D_{\mathrm{lp}}\sin\beta_{\mathrm{lp}}) \end{bmatrix}, \tag{11}$$

$$\vec{M}_{\mathrm{rp}} = \begin{bmatrix} y_{\mathrm{rp}}(L_{\mathrm{rp}}\sin\beta_{\mathrm{rp}} + D_{\mathrm{rp}}\cos\beta_{\mathrm{rp}}) \\ -x_{\mathrm{rp}}(L_{\mathrm{rp}}\sin\beta_{\mathrm{rp}} + D_{\mathrm{rp}}\cos\beta_{\mathrm{rp}}) + z_{\mathrm{rp}}(L_{\mathrm{rp}}\cos\beta_{\mathrm{rp}} - D_{\mathrm{rp}}\sin\beta_{\mathrm{rp}}) \\ -y_{\mathrm{rp}}(L_{\mathrm{rp}}\cos\beta_{\mathrm{rp}} - D_{\mathrm{rp}}\sin\beta_{\mathrm{rp}}) \end{bmatrix}. \tag{12}$$

The hydrodynamic effects on the rigid body that we consider in the dynamic analysis were forces and moments induced by drag. The drag forces are mainly determined by body shape, skin roughness, and flow conditions. To calculate the drag forces, the rigid body is approximated as a rectangular prism, having flow stream normal to three of its faces. The hydrodynamic forces on the body can thus be obtained as follows:

$$\vec{F}_{\mathrm{b}} = \begin{bmatrix} \frac{1}{2}\rho W H C_{Dx} u^2 \\ \frac{1}{2}\rho L H C_{Dy} v^2 \\ \frac{1}{2}\rho L W C_{Dz} w^2 \end{bmatrix} \tag{13}$$

where L, W, and H are the length, the width, and the height of the rigid body, while C_{Dx}, C_{Dy}, and C_{Dz} are drag coefficients of the front, the right, and the bottom faces of the fish body. The hydrodynamic forces on the body also induce hydrodynamic moments that represent the robot's resistance to rotation due to the effective moment arm between the application points and the center of mass. The hydrodynamic moments can be calculated by integrating the infinitesimal moment components due to the drag force around the body. Given the yaw speed r of the robot around z axis, the drag moment resulting from the drag forces in x and y directions are calculated as

$$M_{\mathrm{bz}} = 2\int_0^{\frac{W}{2}} \mathrm{d}M_{\mathrm{bz},x} + 2\int_0^{\frac{L}{2}} \mathrm{d}M_{\mathrm{bz},y} \tag{14}$$

$$= 2\int_0^{\frac{W}{2}} \mathrm{d}F_{\mathrm{b}x}\, y + 2\int_0^{\frac{L}{2}} \mathrm{d}F_{\mathrm{b}y}\, x \tag{15}$$

$$= 2\int_0^{\frac{W}{2}} \frac{1}{2}\rho(H\mathrm{d}y)C_{Dx}(ry)^2 y + 2\int_0^{\frac{L}{2}} \frac{1}{2}\rho(H\mathrm{d}x)C_{Dy}(rx)^2 x \tag{16}$$

$$= \frac{\rho H r^2(C_{Dx}W^4 + C_{Dy}L^4)}{64}. \tag{17}$$

In the same way, the hydrodynamic moments about the x and y axes can be computed. The whole hydrodynamic moments from drag on the rigid body can be represented as

$$\vec{M}_{\mathrm{b}} = \begin{bmatrix} \frac{\rho L p^2(C_{Dy}H^4 + C_{Dz}W^4)}{64} \\ \frac{\rho W q^2(C_{Dx}H^4 + C_{Dz}L^4)}{64} \\ \frac{\rho H r^2(C_{Dx}W^4 + C_{Dy}L^4)}{64} \end{bmatrix}. \tag{18}$$

The net external forces and moments acting on the robot can be obtained by summing up the forces and moments on the body and the propulsors, neglecting the hydrodynamic interactions between them. The translational motions of the robotic fish follow Newton's law and the rotational motions are governed by the Euler's equation. The dynamic model derived from the Newton–Euler motion equation is given by

$$\vec{F} = \mathbf{M}\dot{\vec{v}} + \mathbf{C}(\vec{v})\vec{v}, \tag{19}$$

https://doi.org/10.1017/S0263574709005499 Published online by Cambridge University Press

where $\vec{F}$ is the external force and moment vector, $\mathbf{M}$ is the mass and inertial matrix, $\mathbf{C}(\vec{v})$ is the Coriolis and centripetal terms matrix, and $\vec{v} = [u \quad v \quad w \quad p \quad q \quad r]$ is the translational and rotational velocity vector. When a submerged body is accelerated in water, its surrounding fluid will also be accelerated. These additional forces and moments are described as added mass effect. To compensate the added mass effect, the mass and inertial matrix $\mathbf{M}$ consists not only the mass and inertial matrix $\mathbf{M}_\mathrm{b}$ of the robotic fish but also an added mass and inertial matrix $\mathbf{M}_\mathrm{a}$. Likewise, an added Coriolis and centripetal terms matrix $\mathbf{C}_\mathrm{a}(\vec{v})$ is included in $\mathbf{C}(\vec{v})$. Given the forces and moments acting on the robotic fish, Eq. (19) can be expanded to obtain the equations of the 6-DOF motion as[28]

$$F_x = m(\dot{u} - vr + wq) - X_{\dot{u}}\dot{u} - Z_{\dot{w}}wq + Y_{\dot{v}}vr, \tag{20}$$

$$F_y = m(\dot{v} - wq + ur) - Y_{\dot{v}}\dot{v} + Z_{\dot{w}}wp - X_{\dot{u}}ur, \tag{21}$$

$$F_z = m(\dot{w} - uq + vp) - Z_{\dot{w}}\dot{w} - Y_{\dot{v}}vp + X_{\dot{u}}uq, \tag{22}$$

$$\begin{aligned} M_x = {} & I_{xx}\dot{p} + (I_{zz} - I_{yy})qr - (\dot{r} + pq)I_{xz} + (r^2 - q^2)I_{yz} \\ & + (pr - \dot{q})I_{xy} - L_{\dot{p}}\dot{p} + (Y_{\dot{v}} - Z_{\dot{w}})vw \\ & + (M_{\dot{q}} - N_{\dot{r}})qr, \end{aligned} \tag{23}$$

$$\begin{aligned} M_y = {} & I_{yy}\dot{q} + (I_{xx} - I_{zz})rp - (\dot{p} + qr)I_{xy} + (p^2 - r^2)I_{zx} \\ & + (qp - \dot{r})I_{yz} - M_{\dot{q}}\dot{q} + (Z_{\dot{w}} - X_{\dot{u}})uw \\ & + (N_{\dot{r}} - L_{\dot{p}})pr, \end{aligned} \tag{24}$$

$$\begin{aligned} M_z = {} & I_{zz}\dot{r} + (I_{yy} - I_{xx})pq - (\dot{q} + rp)I_{yz} + (q^2 - p^2)I_{xy} \\ & + (rq - \dot{p})I_{zx} - N_{\dot{r}}\dot{r} + (X_{\dot{u}} - Y_{\dot{v}})uv \\ & + (L_{\dot{p}} - M_{\dot{q}})pq, \end{aligned} \tag{25}$$

where F_x, F_y, F_z, M_x, M_y, and M_z are force or moment components along x, y, z axes, m is the mass of the robotic fish, $X_{\dot{u}}$, $Y_{\dot{v}}$, $Z_{\dot{w}}$, $L_{\dot{p}}$, $M_{\dot{q}}$, and $N_{\dot{r}}$ are partial derivatives of forces or moments with respect to accelerations, I_{xx}, I_{yy}, I_{zz} are the moments of inertia of the robotic fish about x, y, z axes, and I_{xy}, I_{xz}, I_{yz} are the products of inertia. The motion equations are coupled, nonlinear differential equations and the robot states can be obtained through numerical simulations.

3.3. Swimming patterns

Fish in nature exhibits various swimming movements that can be classified into periodic swimming that is characterized by a cyclic repetition of the propulsive movements for a long distance and transient swimming that includes fast start, escape maneuvers, and turns.[3] Both the tail fin and the pectoral fins of the robotic fish can generate propulsion and maneuvering forces and through coordinated control of the propulsors, a great diversity of swimming patterns can be realized. Based upon the propulsors used, the swimming can be classified into two basic modes: BCF mode and MPF mode, although the combined use of tail and pectoral fins can produce more complex movements. Having analyzed the governing dynamics of the robot's motion, several typical swimming patterns can be empirically designed. Figure 6 illustrates the swimming patterns and the realization of each pattern is described as follows:

(1) *BCF forward swimming:* The robotic fish swims in a straight line by oscillating only the tail fin. The angular offset of the tail fin is set to be zero ($\phi_t = 0$) to ensure that the average thrust is directed anteriorly. The oscillations of the pectoral fins are stopped ($A_\mathrm{p} = 0$) and both pectoral fins are held parallel to the horizontal plane functioning to enhance stability ($\phi_\mathrm{p} = 0$).
(2) *BCF turning:* A nonzero offset ϕ_t is superimposed on the oscillation of the tail joint while other parameters remain the same as the BCF forward swimming. The tail fin not only provides the thrust but also produces a nonzero time-averaged torque that will cause a change in heading direction.
(3) *MPF forward and backward swimming:* This swimming pattern can be achieved by the synchronized oscillations of the paired pectoral fins around the horizontal plane, with caudal fin being held straight ($A_\mathrm{t} = 0$, $\phi_\mathrm{t} = 0$). The angular offsets of pectoral fin determine the swimming direction, i.e. $\phi_\mathrm{p} = 0$ for forward swimming and $\phi_\mathrm{p} = 180^\circ$ for backward swimming.
(4) *MPF turning:* The differentiation of hydrodynamic forces between the pectoral fins will cause a yawing moment that is necessary to execute turning maneuvers on the fish body. An effective method to produce the yawing moment is to produce anteriorly directed force on one side and posteriorly directed force on the other side ($\phi_\mathrm{lp} = 180^\circ$, $\phi_\mathrm{rp} = 0^\circ$ or $\phi_\mathrm{lp} = 0^\circ$, $\phi_\mathrm{rp} = 180^\circ$). The oscillation of the tail fin is stopped ($A_\mathrm{t} = 0$, $\phi_\mathrm{t} = 0$).
(5) *Submerging and ascending:* The robotic fish achieves 3D motion by adjusting the attack angle of the pectoral fins like sharks that do not have swim bladders. As a precondition, the robotic fish should attain a swimming speed with BCF or MPF forward swimming pattern. For angular offset ϕ_p between 0° and 90° the force on the pectoral fin can be analyzed into a drag component and a downward lift component, and when ϕ_p is in the range of $(-90^\circ, 0^\circ)$ an upward lift can be generated.
(6) *Braking:* To accomplish braking, fish generate an anteroventrally directed jet by synchronously moving the pectoral fins rapidly out from the body.[4] The robotic fish brakes through rapid and synchronous rotation of the pectoral fins to a position perpendicular to the body ($\phi_\mathrm{p} = 90^\circ$, $A_\mathrm{p} = 0$). The drag caused by the pectoral fin decelerates and eventually stops the motion of the robotic fish.

4. Underwater Vision-based Target Following

4.1. Problem statement

Vision sensors can provide high-resolution information at short range and thus have been extensively used in underwater applications such as marine biology, inspection of power and telecommunication cables, archaeology, and seabed survey.[30] However, the underwater image is plagued by several factors including poor visibility, ambient light, and frequency-dependent scattering and absorption, which make

https://doi.org/10.1017/S0263574709005499 Published online by Cambridge University Press

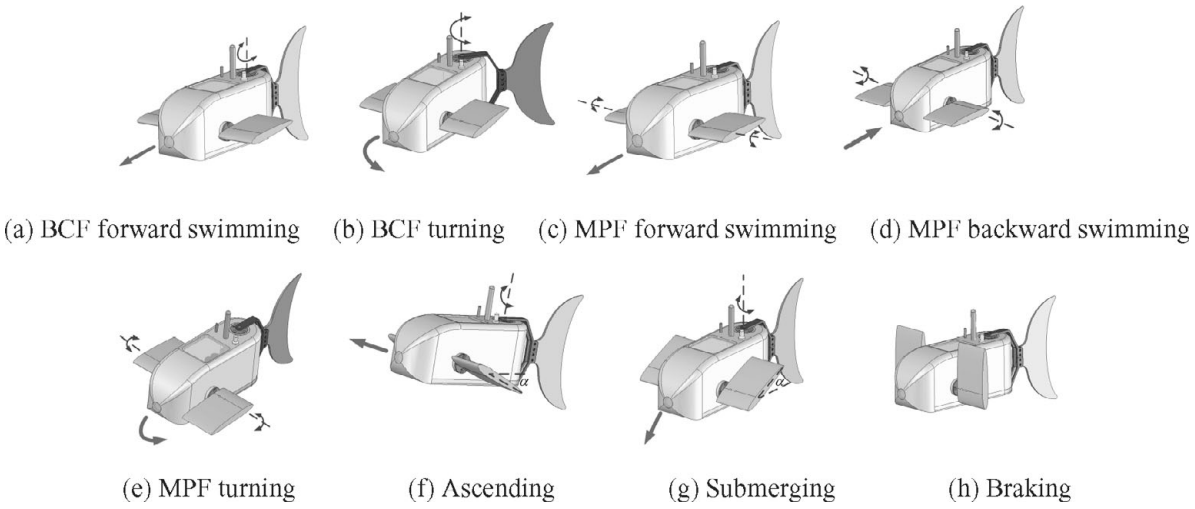

Fig. 6. Illustrations of swimming patterns.

it difficult to directly employ most computer vision methods developed in terrestrial environment. In this research, since the working environment of the robotic fish is indoor shallow water swimming pool, we improve the performance of image processing by providing good lighting conditions as well as employing adaptive and robust computer vision techniques. Besides the low quality of underwater imaging, the complexity of the aquatic environment and peculiarities of the propulsion mode of robotic fish pose several additional difficulties to the successful fulfillment of underwater tasks, which are listed as follows:

- Unlike ground wheeled vehicles instrumented with optical encoders for speed feedback of wheel rotation, the swimming velocity and orientation of robotic fish cannot be precisely controlled and there is no explicit relationship between the motor driving force and the swimming kinematics of the robotic fish.
- The robotic fish cannot stop immediately due to the effect of inertial drift, and even with the swimming pattern of braking and backward swimming to counteract the forward drift the robotic fish will still overshoot slightly.
- Waves occur when the robotic fish flaps to swim, which will affect precise motion planning of the robotic fish. The motion of the robotic fish and the target will be mutually affected through the coupling of waves, which further complicates the problem.

In this research, the robotic fish is required to follow and keep a constant distance to a moving target based on visual feedback from the monocular camera. To avoid possible collision between the target and the robotic fish, the distance is required to be greater than half the body length of the robotic fish, which is approximately the drift distance when the robotic fish stops with braking swimming pattern. Two distinct algorithms have been employed to perform this task. The visual tracking algorithm keeps visual lock on the moving target. The location of the target in image space and the distance between the robot fish and target are obtained in this process. Based on the output of the visual tracking algorithm, the target following algorithm generates motor control commands to keep the target stationary in the center of image and to maintain the distance to the target constant.

4.2. Visual tracking

Visual tracking has been extensively studied in the context of computer vision to find the targets between consecutive frames in image sequences. Numerous algorithms have been proposed and implemented to track moving targets against complex and cluttered background, among which mean shift algorithm has gained considerable attention due to its computational efficiency and robustness to nonrigid deformation.[31] Mean shift algorithm is a nonparametric technique that climbs the gradient of a probability distribution to find the nearest dominant mode. As an adaptation of standard mean shift algorithm, Camshift (Continuously Adaptive Mean Shift) algorithm have been extensively used in practice for head and face tracking.[32] The major challenge to target recognition in underwater visual tracking is the spatially varying degradation effect of visibility, which will cause changes in color probability distributions of the target at different distances. Since the Camshift algorithm can deal with dynamically changing color probability distributions, i.e. distributions are recomputed for each frame, it fits fairly well this underwater target tracking task. In Camshift algorithm, a search window that surrounds the target is employed to specify the location and the size (or scale) of the target. When the target moves in the image plane, the location of the search window will move accordingly, and when the target moves toward the camera, the scale of the target on the image will get bigger, and vice versa. Since the location and distance change of the target can be reflected by the search window, we can actively steer the mobile imaging platform to center the search window in the image and keep its scale constant, so that the target can be followed by the robot.

The Camshift algorithm operates on a probability distribution image that is derived from the histogram of the object to be tracked. The H channel in HSV (Hue Saturation Value) color space is mostly used for calculation of stochastic color model due to its robustness to varying lighting conditions. However, the H components of the image

https://doi.org/10.1017/S0263574709005499 Published online by Cambridge University Press

data are not directly available since the incoming frames are in YCrCb 4:2:2 format, in which a pair of consecutive pixels is represented by one Y (luminance) sample each but share a Cr (red chrominance) sample and a Cb (blue chrominance) sample. To save the computational resources spent on the conversion between color spaces, we modify the standard Camshift algorithm to let it employ Cr and Cb components of the incoming frames to calculate 2D color histogram. The Y component is discarded due to its wild fluctuation in the underwater environment. The principle steps of the Camshift algorithm implemented in this research are stated as follows:

(1) Choose the initial location of the mean shift search window.
(2) Calculate the 2D color histogram within the search window.
(3) Perform back-projection of the histogram to a region of interest (ROI) centered at the search window but slightly larger than the mean shift window size.
(4) Iterate mean shift algorithm to find the centroid of the probability image and store the zeroth moment and centroid location. The mean location within the search window of the discrete probability image is found using moments. Given that $I(x, y)$ is the intensity of the discrete probability image at (x, y) within the search window, the zeroth moment is computed as

$$M_{00} = \sum_x \sum_y I(x, y). \tag{26}$$

The first moment for x and y is

$$M_{10} = \sum_x \sum_y x I(x, y); \qquad M_{01} = \sum_x \sum_y y I(x, y). \tag{27}$$

Then the mean search window location can be found as

$$x_c = \frac{M_{10}}{M_{00}}; \qquad y_c = \frac{M_{01}}{M_{00}}. \tag{28}$$

(5) For the next video frame, center the search window at the mean location stored in Step 4 and set the window's size to a function of the zeroth moment. Go to Step 2. The scale of the target is determined by finding an equivalent rectangle that has the same moments as those measured from the probability distribution image. Define the second moments as

$$M_{20} = \sum_x \sum_y x^2 I(x, y); \qquad M_{02} = \sum_x \sum_y y^2 I(x, y);$$
$$M_{11} = \sum_x \sum_y xy I(x, y). \tag{29}$$

Use the following intermediate variables:

$$a = \frac{M_{20}}{M_{00}} - x_c^2; \qquad b = 2\left(\frac{M_{11}}{M_{00}} - x_c y_c\right);$$
$$c = \frac{M_{02}}{M_{00}} - y_c^2. \tag{30}$$

Then the dimension of the search window can be computed as

$$h = \sqrt{\frac{(a + c) - \sqrt{b^2 + (a - c)^2}}{2}};$$
$$w = \sqrt{\frac{(a + c) + \sqrt{b^2 + (a - c)^2}}{2}}. \tag{31}$$

The mean location and size of the search window is used as output of the visual tracking algorithm. The Camshift algorithm is computationally efficient and can produce real time response to the appearance change of the target. In this research, the motion of the target is restricted in the horizontal plane, so that only x_c of the search window varies as the target moves. For the target that has elongated shape, the scale cannot be reflected exactly by the width of the search window when the target turns, therefore we use height of the search window as the distance clue.

4.3. Target following

Because flapping movements at the tail will produce lateral forces that cause oscillations at the anterior part of the robotic fish where the camera locates, we employ a hybrid swimming pattern for target following. This swimming pattern which has been experimentally validated to produce minimum oscillations at the head, uses synchronized pectoral fins for thrust generation and tail fin as a rudder. The deflection direction of the tail fin produces different rotational effects during forward and backward swimming. For example, the robotic fish turns left with left deflection of the tail fin in forward swimming, while right turning will be effected in backward swimming. As a result, control of the orientation should take into consideration the direction of the translational speed. The intractable nature of the underwater environment makes it difficult to employ classical model-based control method for this task, therefore we regulate the motion of the robotic fish with fuzzy logic control method, which allows management of heuristic rule base knowledge, imprecise information from sensors, and the uncertainties in the knowledge about the environment. The robotic fish regulates its translational and rotational speeds to follow the target, therefore two fuzzy logic controllers are designed, with one for speed control and the other for orientation control. The architecture of the closed-loop control system is illustrated in Fig. 7.

The inputs of the fuzzy logic speed controller are height error e_h of the search window and its change rate Δe_h, which are both measured in terms of pixels and defined as

$$e_h(k) = h_r - h(k); \quad \Delta e_h(k) = e_h(k) - e_h(k - 1) \tag{32}$$

where h_r is the height of the search window at system startup, and k is the discrete time instant. The value of the input variable e_h is fuzzified and expressed by linguist fuzzy sets {VC, C, M, F, VF}, abbreviated from *very close*, *close*, *medium*, *far*, and *very far*, respectively. The initial height of the target window is 60, so that the range of e_h

https://doi.org/10.1017/S0263574709005499 Published online by Cambridge University Press

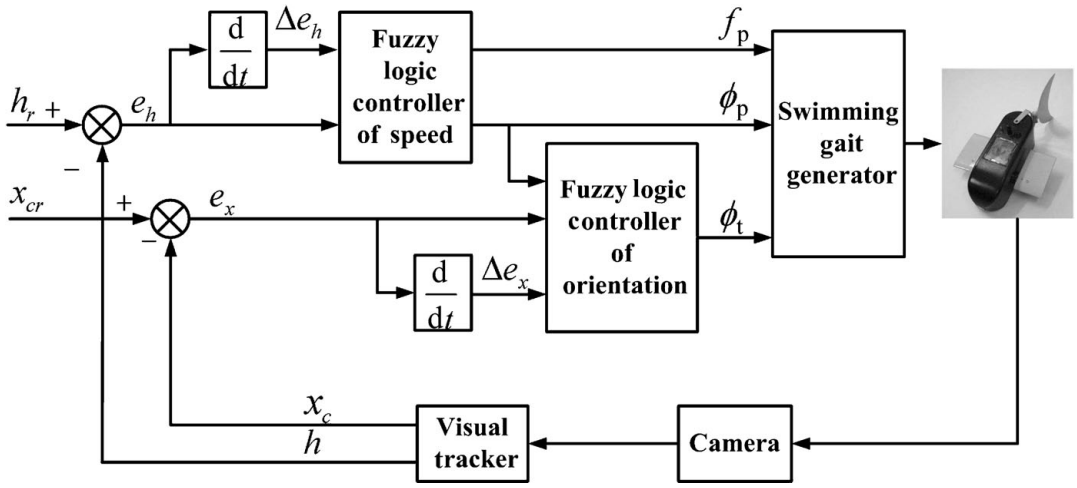

Fig. 7. Closed-loop control system of target following.

is between −180 and 60. The height change rate Δe_h is represented by {NB, NS, ZE, PS, PB}, abbreviated from *negative big*, *negative small*, *zero*, *positive small*, and *positive big*, respectively. The outputs of the speed controller are the oscillatory frequency f_p and angular offset ϕ_p of the pectoral fins. To simplify the problem, the amplitudes of the pectoral fins are held constant and only the oscillatory frequency f_p is used for translational speed control, whereas the angular offset ϕ_p is used for forward and backward direction control. Backward swimming is necessary because the target may suddenly stop or reverse direction and the robotic fish have to swim backwardly to keep distance. The output variable f_p is expressed by the fuzzy sets {Q, S, ST}, denoting *quick*, *slow*, and *stop*, respectively. The driving capacity of the motors determines the range of f_p between 0 and 4 Hz. In practical implementation, the angular offset ϕ_p of the pectoral fins is 0° for forward swimming and 180° for backward swimming. We represent ϕ_p with two singleton fuzzy sets F and B, denoting *forward* and *backward,* respectively. The membership functions of the input and output variables are illustrated in Fig. 8, and the mapping from input variables to output variables is based on the fuzzy rulebase which comprises 25 if-then rules listed in Table I.

Since orientation control of the robotic fish is dependent not only on the deflection direction of tail fin but also on the direction of translational speed, the orientation controller should take the angular offset ϕ_p of the pectoral fins as an input, which has been illustrated in Fig. 7. The other two inputs of orientation controller are the horizontal location error e_x of the search window and its change rate Δe_x, which are defined as

$$e_x(k) = x_{cr} - x_c(k); \qquad \Delta e_x(k) = e_x(k) - e_x(k-1), \tag{33}$$

where x_{cr} is the horizontal coordinate of the image center. The value of the input variable e_x is fuzzified and expressed

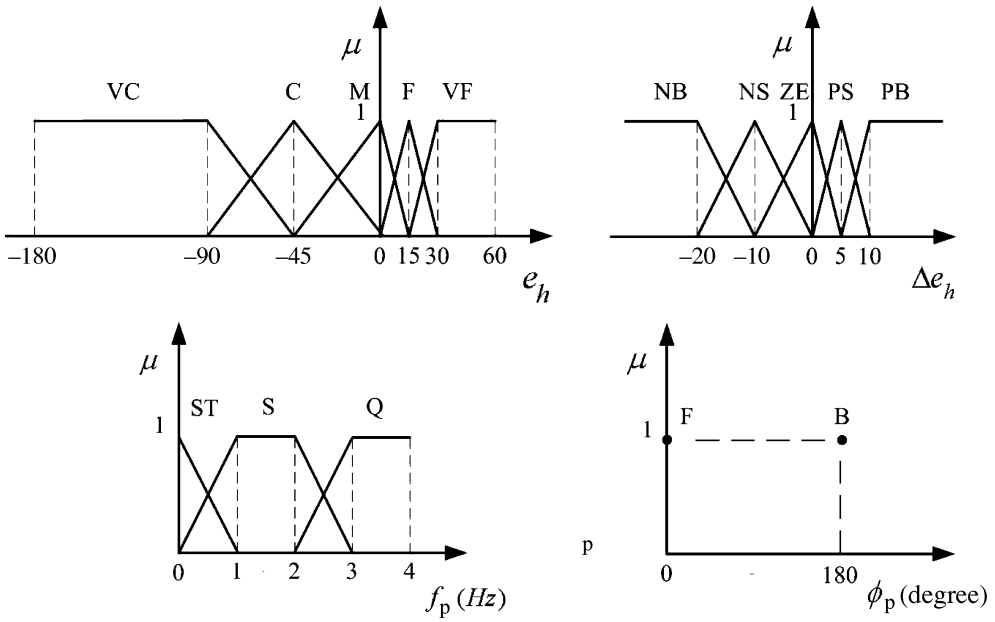

Fig. 8. Membership functions for speed controller.

https://doi.org/10.1017/S0263574709005499 Published online by Cambridge University Press

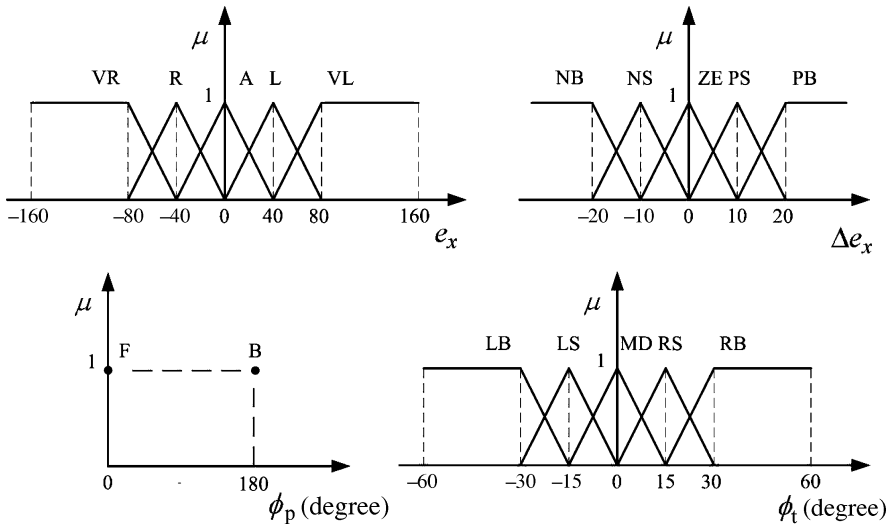

Fig. 9. Membership functions for orientation controller.

Table I. Rulebase for speed controller.

		Δe_h				
f_p, ϕ_p		NB	NS	ZE	PS	PB
e_h	VC	Q, B	Q, B	Q, B	S, B	S, B
	C	Q, B	Q, B	S, B	S, B	S, B
	M	ST, F	ST, F	ST, F	ST, F	ST, F
	F	S, F	S, F	S, F	Q, F	Q, F
	VF	S, F	S, F	Q, F	Q, F	Q, F

Table II. Rulebase for orientation controller.

		Δe_x				
ϕ_t		NB	NS	ZE	PS	PB
e_x	VL	LB	LB	LB	LS	LS
	L	LB	LB	LS	LS	LS
	A	MD	MD	MD	MD	MD
	R	RS	RS	RS	RB	RB
	VR	RS	RS	RB	RB	RB

by the linguist fuzzy sets {VL, L, A, R, VR}, referring to *very left*, *left*, *ahead*, *right*, and *very right*, respectively. The range of the membership function for e_x is between -160 and 160. The change rate Δe_h of horizontal location error is represented by {NB, NS, ZE, PS, PB}, abbreviated from *negative big*, *negative small*, *zero*, *positive small*, and *positive big*, respectively. Like in speed controller, the angular offset ϕ_p is also represented by two singleton fuzzy sets F and B, denoting *forward* and *backward,* respectively. The output of the orientation controller is the angular offset ϕ_t of the tail fin, which is expressed by {LB, LS, MD, RS, RB}, denoting *left big*, *left small*, *middle*, *right small*, and *right big*, respectively. The range of the deflection is between -60° and 60°. Figure 9 shows the membership functions for the orientation controller. The fuzzy rulebase of orientation controller comprises a total of 50 if-then rules. In case of forward swimming, the rules are listed in Table II, while the rules for backward swimming can be easily deduced.

We adopt Mamdani fuzzy inference method, and the crisp value of the output variables are determined using the center-of-gravity (COG) defuzzification method as

$$f_p = \frac{\sum_{k=1}^{25} \mu_k f_p^k}{\sum_{k=1}^{25} \mu_k}; \quad \phi_p = \frac{\sum_{k=1}^{25} \mu_k \phi_p^k}{\sum_{k=1}^{25} \mu_k}; \quad \phi_t = \frac{\sum_{k=1}^{25} \mu_k \phi_t^k}{\sum_{k=1}^{25} \mu_k}, \tag{34}$$

where μ_k is the degree of the "if" part of the kth rule, f_p^k, ϕ_p^k, and ϕ_t^k are the estimated outputs derived from the kth rule, related to the center of the membership functions of the output variables.

5. Experiment

5.1. Experimental setup

Experiments with the robotic fish were carried out in an indoor swimming tank with the size of 2250 mm × 1250 mm and with still water of 350 mm in depth. The robotic fish is marked with specified colors and the information within the swimming tank is captured by an overhead CCD camera. The image is transmitted to a personal computer and processed with a visual tracking software platform developed to obtain the position and orientation of the robotic fish in real time. The 2D trajectory of the robotic fish can also be extracted and recorded for off-line analysis. Figure 10 shows a photograph of the experiment environment.

5.2. Tests of swimming performance

The parameters that characterize the swimming locomotion of the robotic fish constitute a vast variable space which precludes the possibility of a thorough exploration. Hence, experiments were conducted by testing several of the swimming patterns described above. The swimming

https://doi.org/10.1017/S0263574709005499 Published online by Cambridge University Press

Fig. 10. Photograph of the experimental environment.

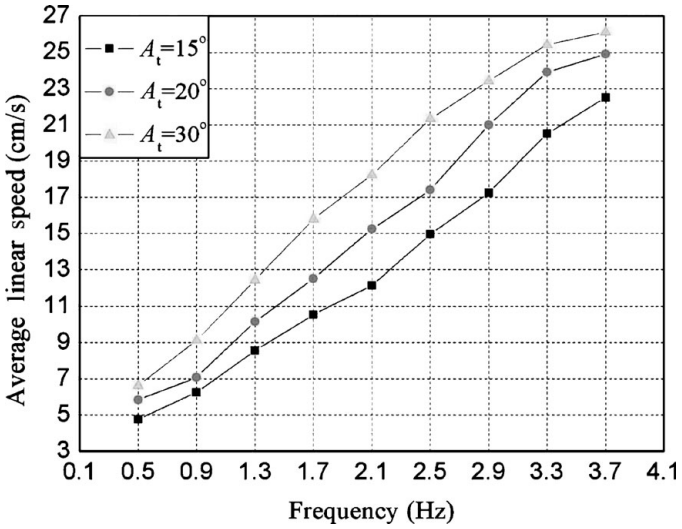

Fig. 11. Average linear speed in BCF forward swimming with different frequencies and amplitudes.

Table III. Swimming performance of BCF turning. Parameters: $A_t = 15°$, $f_t = 2.1$Hz.

ϕ_t (deg)	10	20	30	40
R (cm)	91	63	39	27
ω (rad/s)	0.27	0.41	0.64	0.87

Table IV. Swimming performance of MPF turning. Parameters: $A_p = 20°$.

f_p (Hz)	0.9	1.7	2.5	3.3
R (cm)	8	13	24	41
ω (rad/s)	0.20	0.22	0.21	0.23

performance was tested by tuning the concerned parameters manually while holding the others constant.

For BCF forward swimming pattern, the average linear speed is tested by varying the tail beat frequency and amplitudes. Three groups of amplitudes A_t are employed while the frequency f_t is varied in each case. The swimming

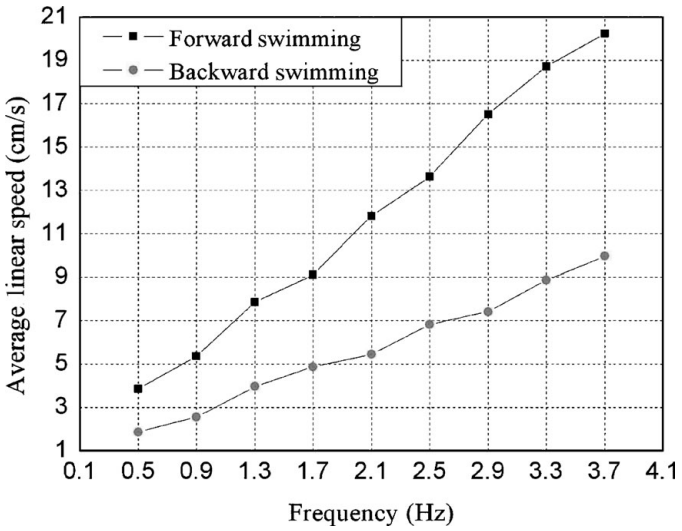

Fig. 12. Average linear speed of MPF forward and backward swimming versus frequency. Parameters: $A_p = 20°$.

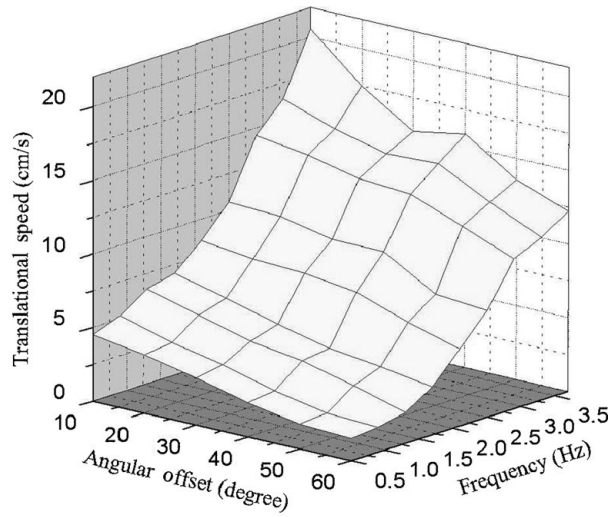

(a) Translational speed in forward swimming.

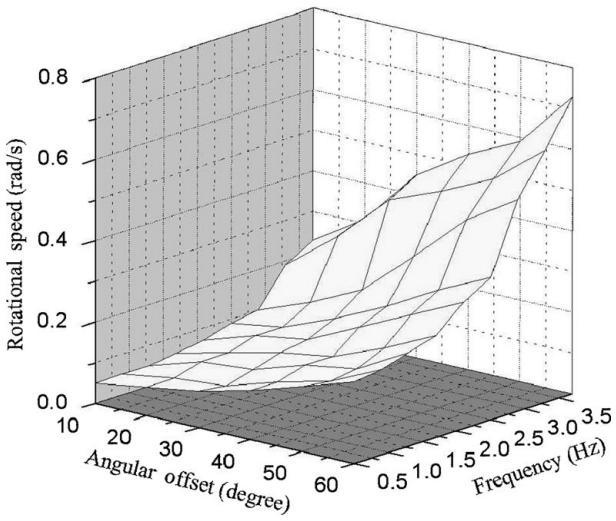

(b) Rotational speed in forward swimming.

Fig. 13. Translational and rotational speeds with different frequencies f_p of both pectoral fins and angular offsets ϕ_t added to the tail joint.

https://doi.org/10.1017/S0263574709005499 Published online by Cambridge University Press

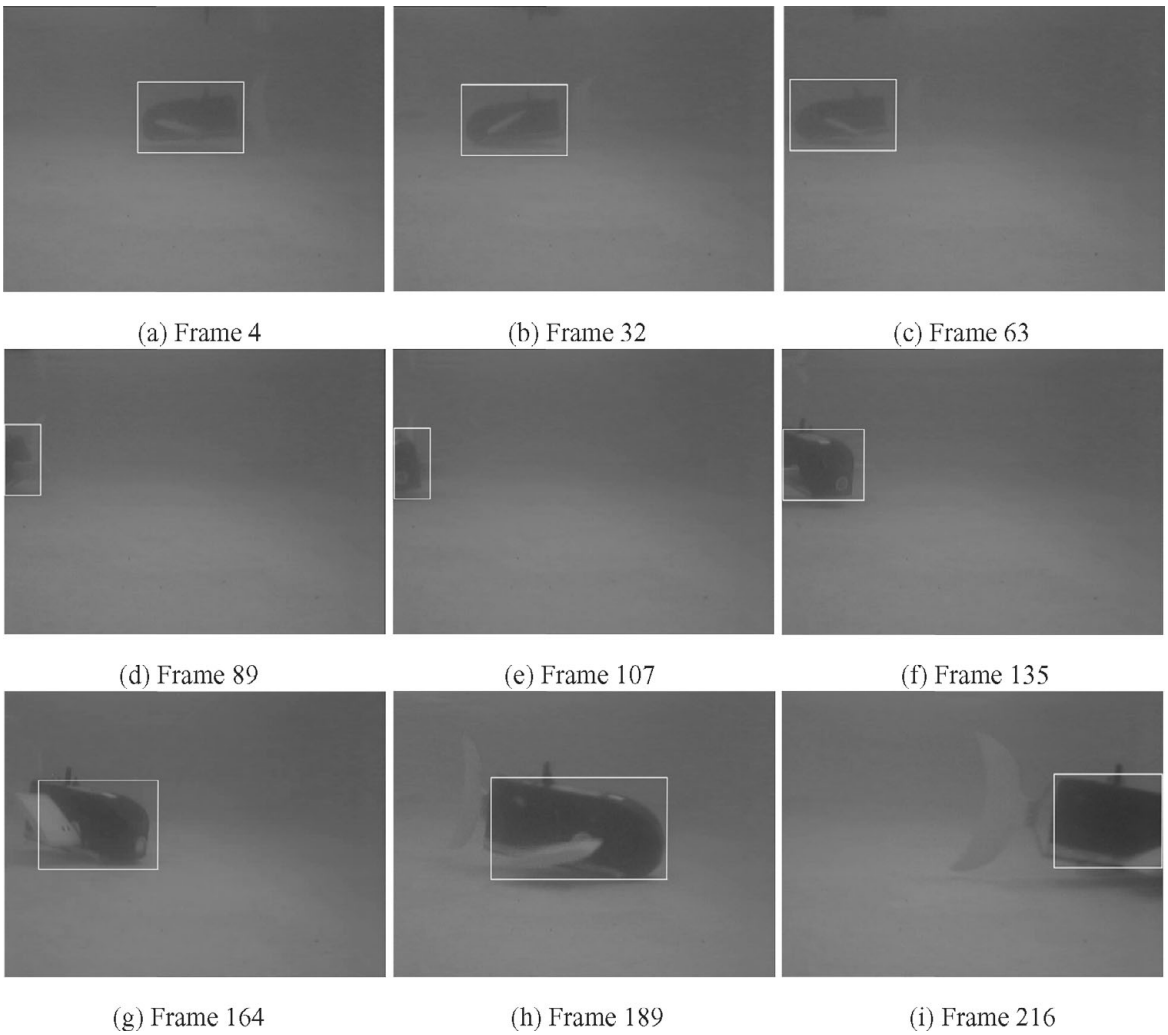

Fig. 14. Tracking results of the swimming sequence with Camshift algorithm.

speed, as illustrated in Fig. 11, increases almost linearly with the frequency, and large amplitude can also provide more thrust. Due to the open-loop property of motor control system, the desired amplitudes cannot be reached at higher frequency, which results in the speed saturation at the performance limits of the servomotors. The maximum speed of BCF forward swimming can reach 26 cm/s, which is approximately 0.74 body length per second. The swimming performance of BCF turning can be evaluated in terms of turning radius R and rotational speed ω. Test results with four different angular offsets ϕ_t added to the tail joint are listed in Table III. According to the experimental data, the turning radius decreases and the turning rate increases with increasing of the angular offset. So that this behavior can be used not only for small course adjustment but also for rapid turn in narrow space.

Tests of MPF-based swimming patterns are carried out by varying the frequency f_p of both pectoral fins, while the amplitudes A_p are kept at constant values. Figure 12 shows the forward and backward swimming speed at different frequencies. As BCF forward swimming, the speeds increase in proportion with the frequency in both cases. However, for the same frequency, the speed of backward swimming is significantly less than that of forward swimming. The performance of MPF turning is tested under different frequencies, with angular offset on one side being 0° and another side being 180°. The experimental results are shown in Table IV.

Particularly, the performance of the hybrid swimming pattern used in target following task is tested for construction of the fuzzy rulebase. The translational and rotational speeds in forward swimming under different frequencies f_p of pectoral fins and angular offset ϕ_t added to the tail joint are shown in Fig. 13.

5.3. Tests of target following

The moving target in the target following experiment is chosen to be another robotic fish which is remotely controlled. The performance of the Camshift algorithm is evaluated on a S3C2440 evaluation board which has LCD interface for image display. The camera is waterproofed and placed in the water, and the robotic fish is commanded to swim in a circle in the swimming pool. The tracking results with stationary camera are shown in Fig. 14. As illustrated in the figure, the algorithm can reliably and accurately tracks the location of the robotic fish, and the distance change can also be reflected by the size variation of the search window.

https://doi.org/10.1017/S0263574709005499 Published online by Cambridge University Press

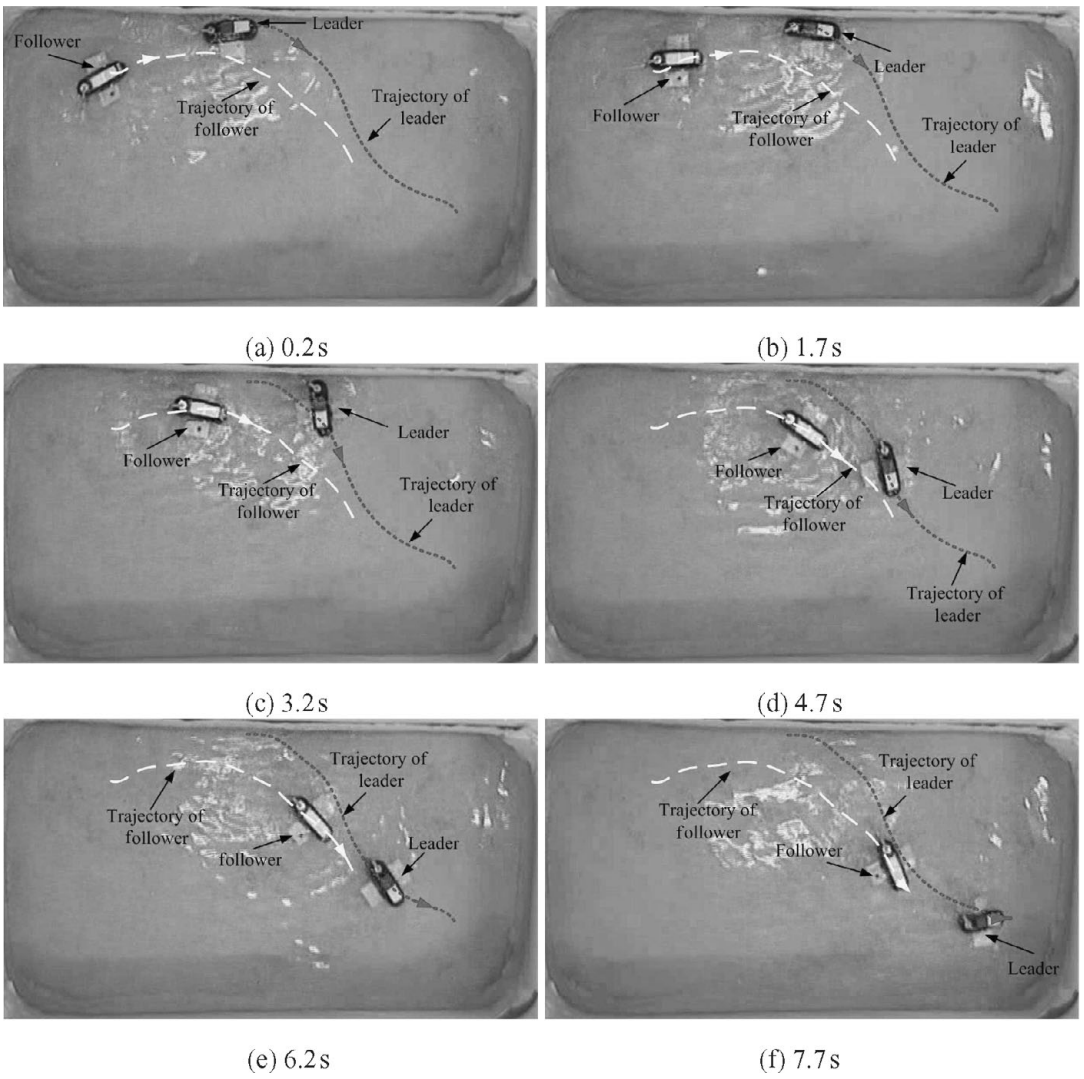

Fig. 15. Scenarios of target following experiment.

The image sequence is processed at a framerate of 30 Hz, occupying approximately 40% of the CPU time.

To facilitate the description, we denote the robotic fish being followed as the leader and the tracking robotic fish as the follower. Both the leader and follower are marked with specified colors, so that the target following results can be captured with the overhead camera and analyzed with the host PC. The initial search window of the follower is located in the center of the image and its initial size is 100×60. At the startup of the following process, the leader is placed in front of the follower and the distance is tuned so that the leader will fit the search window. Control period of the closed-loop control system cannot be so fast as the visual processing rate due to slow response of the robot dynamics. Motor control command is generated every 200 ms based on the measurements of the last five consecutive frames. The data fed into the fuzzy controller $\overline{M}$ is computed with a weighted mean filter

$$\overline{M} = 0.3M_n + 0.25M_{n-1} + 0.2M_{n-2} + 0.15M_{n-3} + 0.1M_{n-4}, \quad (35)$$

where $M_i,\ i = n, n-1, \ldots, n-4$ are the measurements of five consecutive frames within a control interval. Figure 15 shows the scenarios of target following experiment. The trajectories in the figures illustrate that the follower can detect the position and distance changes of the leader and follow the leader as it swims with varying speed and in different directions. However, due to the complexity of the underwater environment and the peculiarities of the robot's locomotion mode, the distance between the leader and the follower fluctuates to some extent rather than remains at a constant value. The maximum distance error occurs when the leader executes turning maneuvers and the follower has to brake in order to keep distance. Figure 16 shows the distance between the leader and the follower over time.

6. Conclusions and Future Work

This paper was concerned with the development and target following of an ostraciiform swimming, vision-based autonomous robotic fish. Design details including the mechanical configurations, electronics, sensor, and software

https://doi.org/10.1017/S0263574709005499 Published online by Cambridge University Press

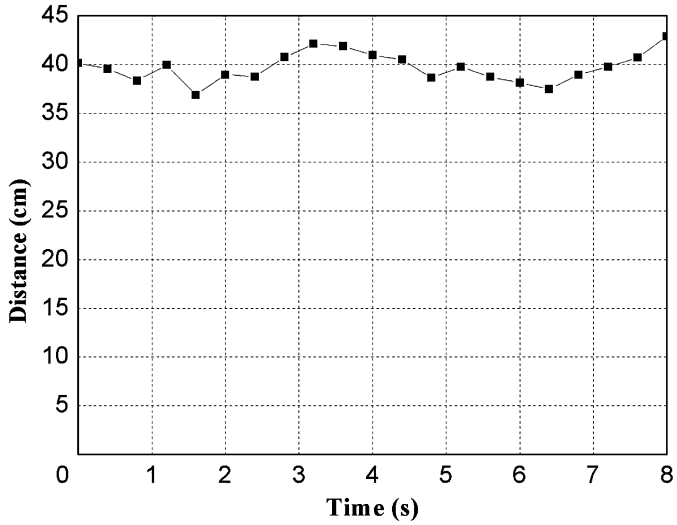

Fig. 16. The distance between the leader and the follower over time.

were described. The algorithm for swimming locomotion control, dynamic analysis of its motion, and the design of various swimming patterns were presented. The target following task was addressed with modified Camshift algorithm for visual tracking and fuzzy logic controller for motion regulation. Experiments were conducted to test the swimming performance of the robotic fish and to verify the effectiveness of the proposed method.

In this paper, the target following task was performed in the horizontal plane. In the case of 3D following, the vertical center of the search window can be used as another input of the motion controller, and the angular offsets of the pectoral fins can be adjusted to regulate the depth of the robotic fish. Future work with the robotic fish will be carried out in three aspects. First, the dynamic model of the robotic fish will be verified through simulation and comparison of the simulated and experimental results. Second, the pectoral fin which plays an important role in ostraciiform swimming should be improved to incorporate more degrees of freedom, allowing more dexterous swimming of the robotic fish. Third, since the capability of a single robotic fish is often limited, coordinated control of multiple robotic fish is an appealing approach to address more complex underwater missions such as large object manipulation, cooperative military detection, and seabed exploration. For use of the robotic fish in real-world applications, more technical hurdles such as reliable underwater communication, high transit speed, long range and duration should be addressed in the long term.

Acknowledgments

This work was supported by National 863 Program (2006AA04Z258), NSFC (60674050 and 60528007), 11-5 project (A2120061303), and National 973 Program (2002CB312200). The authors would like to thank the referees for careful reading of the manuscript and for their helpful comments.

References

1. P. R. Bandyopadhyay, "Trends in biorobotic autonomous undersea vehicles," *IEEE J. Oceanic Eng.* **30**(1), 109–139 (2005).
2. F. E. Fish and G. V. Lauder, "Passive and active flow control by swimming fishes and mammals," *Annu. Rev. Fluid Mech.* **38**, 193–224 (2006).
3. M. Sfakiotakis, D. M. Lane and J. Bruce C. Davies, "Review of fish swimming modes for aquatic locomotion," *IEEE J. Oceanic Eng.* **24**(2), 237–252 (1999).
4. G. V. Lauder and E. G. Drucker, "Morphology and experimental hydrodynamics of fish fin control surfaces," *IEEE J. Oceanic Eng.* **29**(3), 556–571 (2004).
5. G. V. Lauder and E. D. Tytell, "Hydrodynamics of undulatory propulsion," *Fish Biomech.* **23**, 425–468 (2006).
6. M. W. Westneat, D. H. Thorsen, J. A. Walker and M. E. Hale, "Structure, function and neural control of pectoral fins in fishes," *IEEE J. Oceanic Eng.* **29**(3), 674–683 (2004).
7. M. S. Triantafyllou and G. S. Triantafyllou, "An efficient swimming machine," *Sci. Am.* **272**(3), 64–70 (1995).
8. D. Barrett, M. Grosenbaugh and M. Triantafyllou, "The Optimal Control of a Flexible Hull Robotic Undersea Vehicle Propelled by an Oscillating Foil," *Proceedings of 1996 IEEE AUV Symposium* (Monterey, CA, 1996) pp. 1–9.
9. J. M. Anderson and P. A. Kerrebrock, "The Vorticity Control Unmanned Undersea Vehicle (VCUUV)—An Autonomous Vehicle Employing Fish Swimming Propulsion and Maneuvering," *Proceedings of 10th International Symposium on Unmanned Untethered Submersible Technology* (Durham, New Hampshire, 1997) pp. 189–195.
10. R. Mason and J. Burdick, "Experiments in Carangiform Robotic Fish Locomotion," *Proceedings of International Conference on Robotics and Automation* (San Francisco, CA, 2000) pp. 428–435.
11. T. Hirata, Welcome to fish robot home page (2000). Available at: http://www.nmri.go.jp/eng/khirata/fish/.
12. J. Liu, H. Hu and D. Gu, "A Hybrid Control Architecture for Autonomous Robotic Fish," *Proceedings of International Conference on Intelligent Robots and Systems* (Beijing, 2006) pp. 312–317.
13. N. Kato, "Control performance in the horizontal plane of a fish robot with mechanical fins," *IEEE J. Oceanic Eng.* **25**(1), 121–129 (2000).
14. K. H. Low, "Locomotion Consideration and Implementation of Robotic Fish with Modular Undulating Fins: Analysis and Experimental Study," *Proceedings of International Conference on Intelligent Robots and Systems* (Beijing, 2006) pp. 2424–2429.
15. Y. Hu, L. Wang, W. Zhao, Q. Wang and L. Zhang, "Modular Design and Motion Control of Reconfigurable Robotic Fish," *Proceedings of International Conference on Decision and Control* (New Orleans, LA, 2007) pp. 5156–5161.
16. F. E. Fish, G. V. Lauder, R. Mittal, A. H. Techet, M. S. Triantafyllou, J. A. Walker and P. W. Webb, "Conceptual Design for the Construction of a Biorobotic AUV Based on Biological Hydrodynamics," *Proceedings of 13th International Symposium on Unmanned Untethered Submersible Technology*, New Hampshire (Durham, New Hampshire, 2003).
17. J. E. Colgate and K. M. Lynch, "Mechanics and control of swimming: A review," *IEEE J. Oceanic Eng.* **29**(3), 660–673 (2004).
18. S. D. Kelly, R. J. Mason, C. T. Anhalt, R. M. Murray and J.W. Burdick, "Modeling and Experimental Investigation of Carangiform Locomotion for Control," *Proceedings of American Control Conference* (Philadelphia, PA, 1998) pp. 1271–1276.
19. K. A. McIsaac and J. P. Ostrowski, "Experiments in Closed-Loop Control for an Underwater Eel-Like Robot," *Proceedings of IEEE International Conference on Robotics Automation* (Washington, DC, 2002) pp. 750–755.
20. K. A. Morgansen, T. M. La Fond and J. X. Zhang, "Agile Maneuvering for Fin-Actuated Underwater Vehicles," *Proceedings of International Symposium on Communications, Control and Signal Processing* (Marrakech, Morocco, 2006).

21. J. Yu, L. Wang and M. Tan, "Geometric optimization of relative link lengths for biomimetic robotic fish," *IEEE Trans. Robot.* **23**(2), 382–386 (2007).
22. D. Zhang, L. Wang, J. Yu and M. Tan, "Coordinated transport by multiple biomimetic robotic fish in underwater environment," *IEEE Trans. Control Syst. Technol.* **15**(4), 658–671 (2007).
23. M. Gordon, J. Hove, P. Webb and D. Weihs, "Boxfishes as unusually well-controlled autonomous underwater vehicles," *Physiol. Biochem. Zool.* **74**(6), 663–671 (2000).
24. J. R. Hove, L. M. OBryan, M. S. Gordon, P. W. Webb and D. Weihs, "Boxfishes (teleostei: Ostraciidae) as a model system for fishes swimming with many fins: Kinematics," *J. Exp. Biol.* **204**(8), 1459–1471 (2001).
25. P. Kodati and X. Deng, "Experimental Studies on the Hydrodynamics of a Robotic Ostraciiform Tail Fin," *Proceedings of International Conference on Intelligent Robots and Systems* (Beijing, 2006) pp. 5418–5423.
26. D. Lachat, A. Crespi and A. J. Ijspeert, "Boxybot: A Swimming and Crawling Fish Robot Controlled by a Central Pattern Generator," *Proceedings of IEEE/RAS-EMBS International Conference on Biomedical Robotics and Biomechatronics* (Pisa, Tuscany, 2006) pp. 643–648.
27. G. V. Lauder and P. G. A. Madden, "Learning from fish: Kinematics and experimental hydrodynamics for roboticists," *Int. J. Automat. Comput.* **3**(4), 325–335 (2006).
28. T. Fossen, *Guidance and Control of Ocean Vehicles* (John Wiley & Sons Ltd., Chichester, UK 1994).
29. A. J. Healey, S. M. Rock, S. Cody, D. Miles and J. P. Brown, "Toward an improved understanding of thruster dynamics for underwater vehicles," *IEEE J. Oceanic Eng.* **20**(4), 354–361 (1995).
30. D. M. Kocak and F. M. Caimi, "The current art of underwater imaging—with a glimpse of the past and vision of the future," *Marine Technol. Soc J.* **39**(3), 5–26 (2005).
31. D. Comaniciu, V. Ramesh and P. Meer, "Kernel-based object tracking," *IEEE Trans. Pattern Anal. Mach. Intell.* **25**(5), 564–575 (2003).
32. G. R. Bradski, "Computer video face tracking for use in a perceptual user interface," *Intel Technol. J.* (1998) (2nd Quarter).

https://doi.org/10.1017/S0263574709005499 Published online by Cambridge University Press